



Trans. Nonferrous Met. Soc. China 31(2021) 2479-2492

Transactions of Nonferrous Metals Society of China

www.tnmsc.cn



# A novel technology of high-voltage pulse discharge for comminution of galena ore

Yong-hong QIN<sup>1,2</sup>, Peng GAO<sup>1,2</sup>, Shuai YUAN<sup>1,2</sup>, Ning-yu ZHANG<sup>1,2</sup>, Li-ren HAN<sup>1,2</sup>

- 1. College of Resources and Civil Engineering, Northeastern University, Shenyang 110819, China;
- National-local Joint Engineering Research Center of High-efficient Exploitation Technology for Refractory Iron Ore Resources, Shenyang 110819, China

Received 9 July 2020; accepted 30 January 2021

**Abstract:** An innovative technology of high-voltage pulse discharge (HVPD) was proposed to investigate the comminution characteristics of galena ore. The optimal experiment parameters were determined as follows: spark gap spacing of 25 mm, pulse number of 120, and voltage of 25 kV. The mass fraction with size <0.074 mm in ground products was improved by the HVPD. Meanwhile, the relative grindability declined with the increase of the grinding time, which indicated that the superiority of HVPD was weakened. The ground products of HVPD were distributed more homogeneously than those of mechanical crushing. The liberation of breakage products was improved by 24.57% via the HVPD. Moreover, the Brunauer–Emmett–Teller (BET) specific surface area, pore volume, and average pore size were increased via the HVPD. Scanning electron microscopy (SEM) and energy-dispersive X-ray spectroscopy (EDS) analyses suggested that obvious grain-boundary breakage and several stomatal traces were observed in the HVPD products.

Key words: galena ore; high-voltage pulse discharge; liberation; microstructure; grain-boundary breakage

#### 1 Introduction

As a vital nonferrous metal, lead is widely used in lead-acid batteries, cables, building materials, radioactivity protection, and other fields. However, the shortage of lead concentrate was about  $1\times10^5$  t in 2017, and there is a serious resource crisis of lead in China [1,2]. Therefore, it is significant to improve the comprehensive utilization of lead resources. However, the lead ores mainly have the characteristics such as low-grade, intergrowth, and fine disseminated grain size. The beneficiation of lead ores in China confronts the challenge of complex co-associated relationships, difficult separation of lead, multiple technological processes, and high processing costs [1,2]. Among them, the crucial problems in the field of ore

comminution are high investment cost of comminution equipment, high energy consumption, and overmuch untreatable fine particle size, and the difficulty of subsequent separation operations was increased.

Several pretreatment approaches proposed to optimize the mineral processing operation, such as coal-based reduction [3], magnetization roasting [4–6], magnetic pulse [7], high-voltage pulse discharge (HVPD) microwave [9,10], and high-pressure roller [11]. HVPD is a typical technique of electric breakdown. The input voltage is stored for a long time, and then the energy is transformed and released to the loading facility in a short time (0-500 ns) to produce the pulse signal with high-density power. Generally, the ores are placed in the insulation fluid (water or transformer oil), and the electrode contacts closely with the ores. When the rising time of voltage is smaller than 500 ns, the breakdown strength of water is higher than that of ores. Hence, water plays the role of a dielectric during the HVPD [12].

The positive effects of HVPD on improving the grinding efficiency and enhancing liberation characteristic have been investigated in recent years [13,14]. Some scholars pointed out that the liberations of porphyry copper, photovoltaic circuit board, and quartz were improved by the HVPD [15-17]. CHANTURIYA et al [18] testified that the contact area between leaching agents and ores was increased via the HVPD to enhance the leaching efficiency. Some scholars found the pre-weakening effects of HVPD on the magnetite quartzite, copper ore, and gold ore by establishing model [19-21]. Besides, DIAO et al [22,23] considered that most coppers of the circuit board were enriched in a narrow range of granularity via the HVPD. ZHAO et al [24] pointed out that the HVPD products had the fractal characteristics of particle size. To date, the researches of galena have focused on the flotation separation among galena, chalcopyrite, sphalerite, pyrite, and molybdenite. However, there were few investigations on the comminution characteristics of galena ore. As a preparation operation of raw material, comminution plays an important role in the mineral processing. Therefore, it is vital to investigate the comminution characteristics of galena ore via the HVPD.

In the present study, the ore sample was a typical lead ore of polymetallic intergrowth. Based on the mineral compositions, contents, and disseminated size of the ore samples, the effects of spark gap spacing, pulse number, and voltage on the comminution characteristics of galena ore were evaluated. The particle size distribution and liberation were studied to evaluate the superiority of HVPD. Moreover, the specific surface area, pore

characteristics, and morphology of comminution products were investigated. According to the comminution characteristics of two breakage approaches, the superiority of HVPD was verified.

#### 2 Experimental

#### 2.1 Materials

The ore sample was collected from a beneficiation plant in Liaoning Province, China. The chemical composition of galena ore was shown in Table 1, which indicated that the useful elements were lead, sulfur, and silver. The contents of lead, sulfur, and silver were 4.38%, 11.10%, and 115.7 g/t, respectively. The mass fractions of impurities CaO, SiO<sub>2</sub>, and MgO were 18.55%, 16.18%, and 13.42%, respectively. The mineral compositions, contents, and disseminated sizes of the ore samples were analyzed by mineral liberation analyzer (MLA). The mineral quantitative analysis results and disseminated size characteristics of the galena ore were summarized in Table 2 and Table 3, respectively. The microstructural characteristics of the galena ore were shown in Fig. 1.

As shown in Table 2, the main metallic minerals in the ore were galena and pyrite, and their mass fractions were 5.06% and 17.57%, respectively. The other metallic minerals included magnetite, chalcopyrite, freibergite, and boulangerite. Gangue minerals mainly consisted of dolomite (57.78%) and quartz (11.38%). Besides, other gangue minerals were mica, calcite, chlorite,

**Table 1** Results of chemical component detection of galena ore (wt.%)

<u> </u>		,				
Pb	TFe	S	As	Ag*	Au*	Cu
4.38	8.20	11.10	0.078	115.7	0.37	0.035
Zn	SiO <sub>2</sub>	$Al_2O_3$	MgO	CaO	K	Na
< 0.01	16.18	3.42	13.42	18.55	0.97	0.05
* g/t						

Table 2 Results of mineral quantitative detection of galena ore (wt.%)

	1	0 (			
Galena	Pyrite	Dolomite	Quartz	Mica	Chlorite
5.06	17.57	57.78	11.38	6.16	0.89
Magnetite	Chalcopyrite	Albite	Rutile	Freibergite	Calcite
0.18	0.04	0.06	0.07	0.06	0.42
Apatite	Arsenopyrite	Boulangerite	Calcite	Stannite	Sphalerite
0.13	0.03	0.03	0.42	0.02	0.05

**Table 3** Disseminated grain sizes of main metallic minerals

Carin sime/www			Prop	ortion/%			
Grain size/μm	Boulangerite	Freibergite	Galena	Mica	Dolomite	Pyrite	Quartz
500-1000	0	0	20.36	25.59	28.38	12.52	17.45
300-500	0	0	22.43	16.23	23.95	22.37	25.22
150-300	0	0	22.01	15.97	16.82	25.91	18.85
75-150	20.95	4.41	13.05	13.06	11.85	17.42	13.57
38-75	34.54	13.45	10.36	13.58	11.31	14.11	13.06
20-38	16.28	26.09	5.59	7.43	4.94	5.08	6.39
10-20	9.77	25.88	2.91	4.55	1.86	1.71	3.41
<10	18.46	30.17	3.29	3.59	0.89	0.88	2.05
Total	100	100	100	100	100	100	100

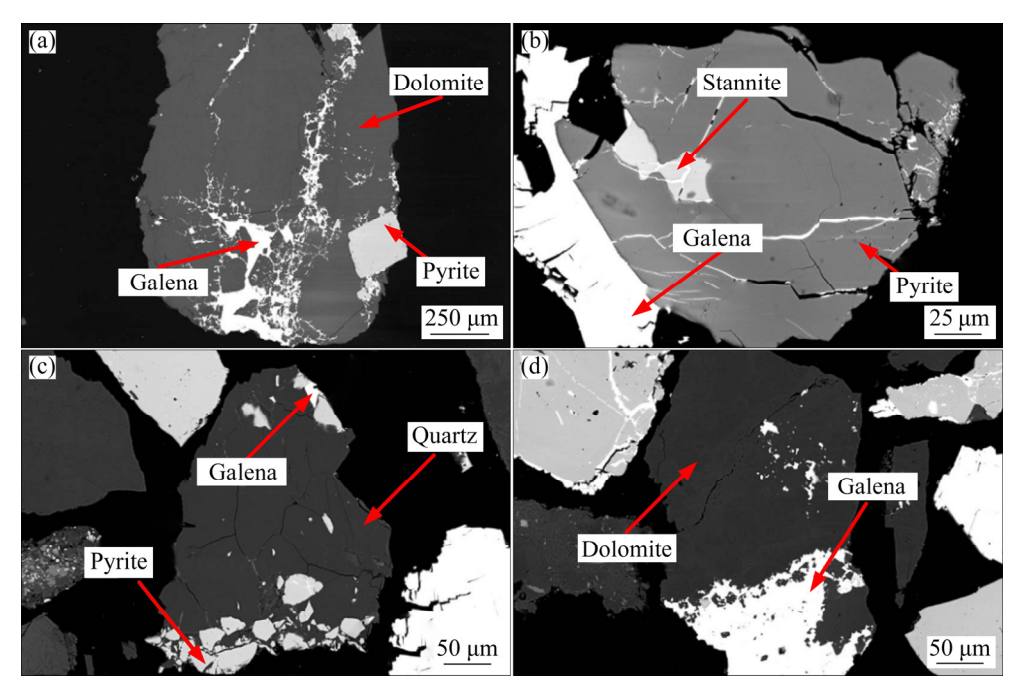


Fig. 1 Microstructural characteristics of galena ores: (a) Galena, dolomite and pyrite; (b) Galena, stannite and pyrite; (c) Galena, quartz and pyrite; (d) Galena and dolomite

and apatite. Figure 1 indicated that galena coexisted closely with other sulfides; meanwhile, galena and pyrite were wrapped by dolomite and quartz, which were unfavorable for the liberation and utilization of metallic minerals.

Table 3 suggested the distribution rates of galena and pyrite in size interval higher than 75  $\mu$ m were 77.85% and 78.22%, respectively. The distribution rates of dolomite, quartz, and mica in size interval higher than 75  $\mu$ m were 81.00%, 75.09%, and 70.85%, respectively. The distribution rates of boulangerite and freibergite in size interval lower than 75  $\mu$ m were 79.05% and 95.59%, which indicated that the disseminated grain sizes of boulangerite and freibergite were fine.

#### 2.2 Experimental approach

The HVPD experiments were operated by a kind of laboratory-scale equipment, and the experiment flow chart was shown in Fig. 2. The HVPD apparatus was designed by scholars from Northeastern University and Shenyang Ligong University, China, which mainly comprised a high-voltage power, a spark gap, a discharge chamber, and a needle-to-plate electrode. 15 g galena ore (5–7 mm) and deionized water were placed in the discharge chamber before pulse discharge. Meanwhile, suitable parameters were set to operate the discharge experiment. At the end of experiments, the samples were dried and sieved using standard screeners with pore size of 2, 1, 0.5

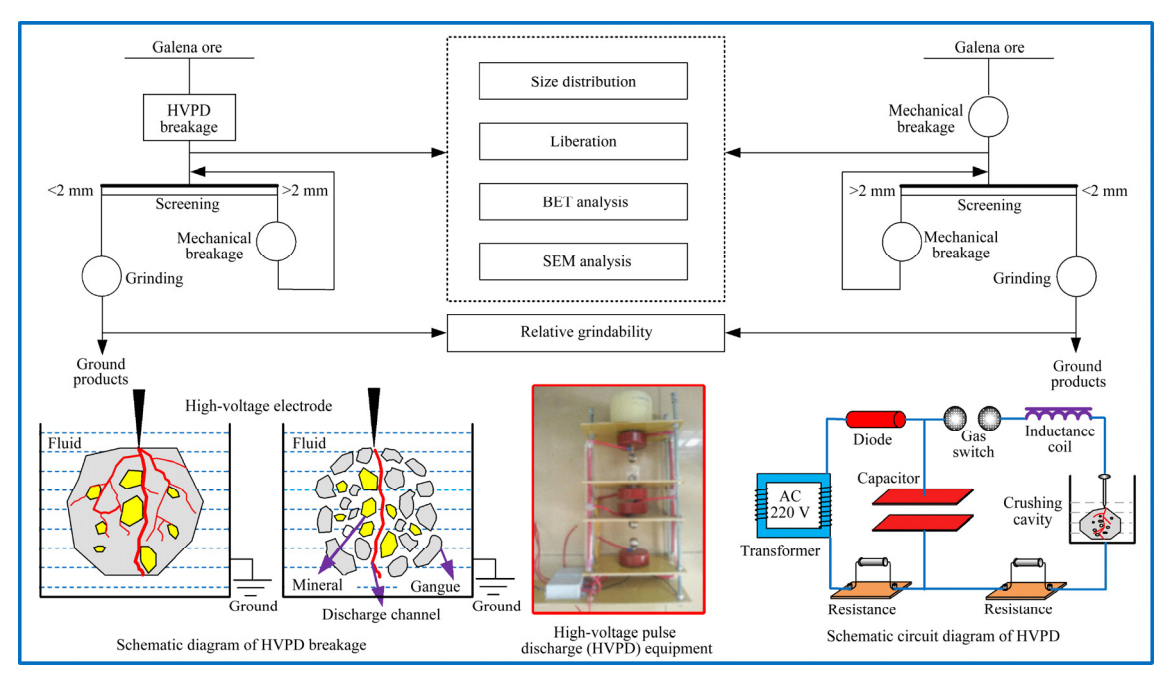


Fig. 2 Experiment flow chart of HVPD pre-treatment

and 0.15 mm, respectively. The coarse products (>2 mm) were broken in a disc crusher (SB200, Germany). 30 g comminution products (<2 mm) were ground in a barrel rod mill (XMB-70-II, China) at grinding pulp concentration of 70 wt.% and grinding time of 15, 30, 45, 60, and 75 s, respectively. The ground products were sieved using a standard screen with a pore size of 0.074 mm. Three times experiments were performed to reduce the experimental errors.

#### 2.3 Analytical method

#### 2.3.1 Scanning electron microscopy analysis

The apparent morphologies of the ore samples were observed under a scanning electron microscope (ULTRA PLUS, Zeiss, Germany). Based on the energy of the X-ray produced by the interaction of the focused electron beam and the samples, the element compositions of the ore samples were obtained via EDS. Since the ore samples had no conductivity, the Au film with a thickness of 10 nm was coated on the sample surface. The microtopography of the ores, energy spectrum of each phase, and element contents were obtained by scanning samples at different magnifying powers and an acceleration voltage of 30 kV.

#### 2.3.2 Liberation analysis

The liberation of mineral was defined as follows: the ratio of the number of liberated

particles to the total number of particles containing the minerals in the group, as shown in Eq. (1):

$$F = \frac{f}{\sum f_i} \tag{1}$$

where F represented the liberation of the mineral; f was the number of liberated particles;  $\sum f_i$  was the total number of particles in the group.

The numbers of conjoined grain with different mineral ratios (0, 1/8, 1/4, 3/8, 1/2, 5/8, 3/4, 7/8, 1) were counted. In this experiment, the particles number of breakage samples observed under optical microscope was 500.

#### 2.3.3 Brunauer-Emmett-Teller analysis

Generally, the pores properties of the solid materials were investigated by the physical adsorption approach such as the BET analysis. The high purity  $N_2$  was inexpensive and available. The II and IV adsorption isotherms were generated on the surfaces via  $N_2$  adsorption. Therefore, 110 data points of adsorption and desorption, the specific surface area, adsorption—desorption curve, and the pore distribution parameters were obtained via the  $N_2$  adsorption (ASAP 2460, American).

#### 3 Results and discussion

## 3.1 Effect of HVPD parameters on comminution of galena ore

#### 3.1.1 Spark gap spacing

The effect of spark gap spacing on comminution characteristics was studied at a spark gap spacing varying from 15 to 30 mm, a pulse number of 120, and a voltage of 25 kV. The pulse energy was 0.972 kW·h/t. The mass fractions of HVPD products at different spark gap spacings were shown in Fig. 3.

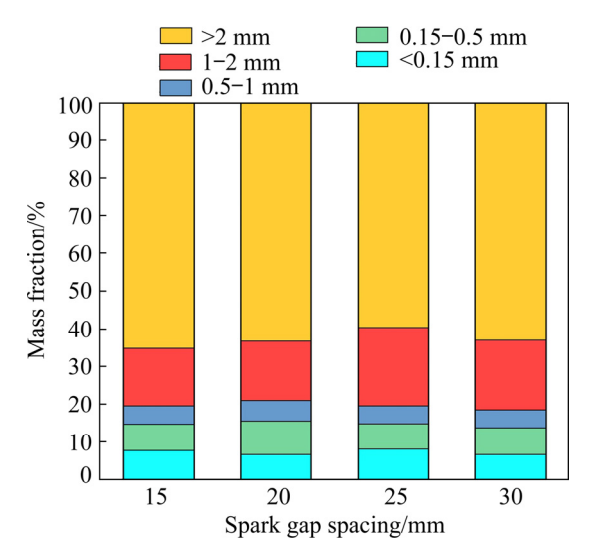


Fig. 3 Particle size distribution at different spark gap spacings

Figure 3 indicated that the mass fraction of HVPD products with size less than 2 mm increased to the peak value (40.01%) at a spark gap spacing of 25 mm, and that at a spark gap spacing of 15 mm was 34.86%. The spark gap was a trigger in the HVPD experiment. The spark gap spacing was inversely proportional to the electric field intensity in the spark gap, as shown in Eq. (2):

$$U=Ed$$
 (2)

where U was voltage (kV); E was the electric field intensity (A/m); d was the distance between spark gap (m).

At the same voltage, the larger distance of spark gap represented the smaller electric field intensity. The rising time of voltage was controlled by the spark gap spacing, and the longer rising time of voltage was produced by the larger spacing of spark gap. Meanwhile, the pulse frequency was inversely proportional to the spark gap spacing. The accelerated pulse frequency was not conducive for storing and releasing electric energy, which was also disadvantageous to the comminution of galena ore. The spark gap spacing was determined to be 25 mm.

The coarse HVPD products (>2 mm) were broken to <2 mm by mechanical breakage for the grinding experiment, as shown in Fig. 4. At a spark gap spacing of 15 mm, the mass fractions of 1–2, 0.5–1, 0.3–0.5, 0.15–0.3, 0.074–0.15, and <0.074 mm were 39.59%, 24.88%, 6.85%, 12.16%, 6.24%, and 9.75%, respectively.

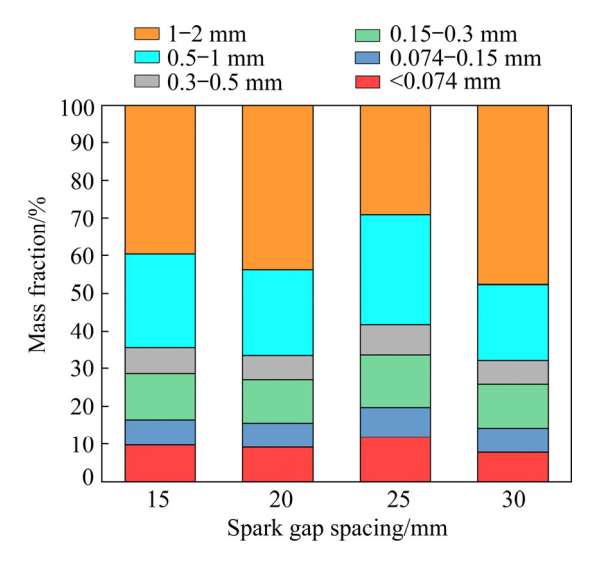


**Fig. 4** Feed size distribution in ball mill at different spark gap spacings

#### 3.1.2 Pulse number

The effect of pulse number on comminution characteristic was investigated at a pulse number between 30 and 150, a spark gap spacing of 25 mm, and a voltage of 25 kV. The mass fractions of HVPD products at different pulse numbers were shown in Fig. 5. The energy was listed in Table 4.

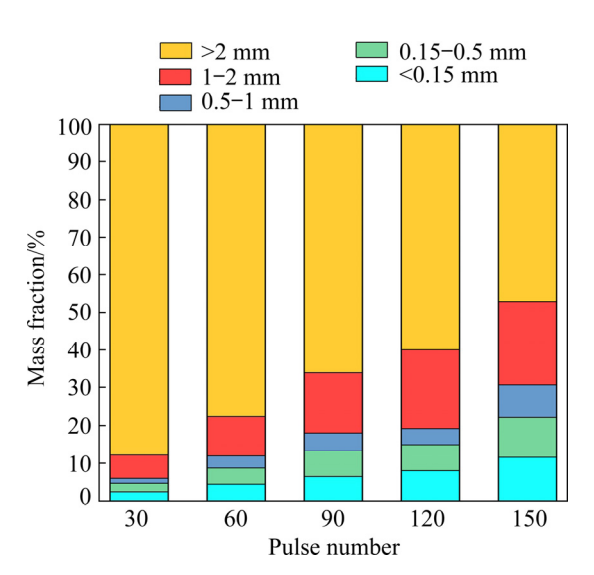


**Fig. 5** Particle size interval productivity at different pulse numbers

**Table 4** Energy of HVPD pre-treatment at different pulse number

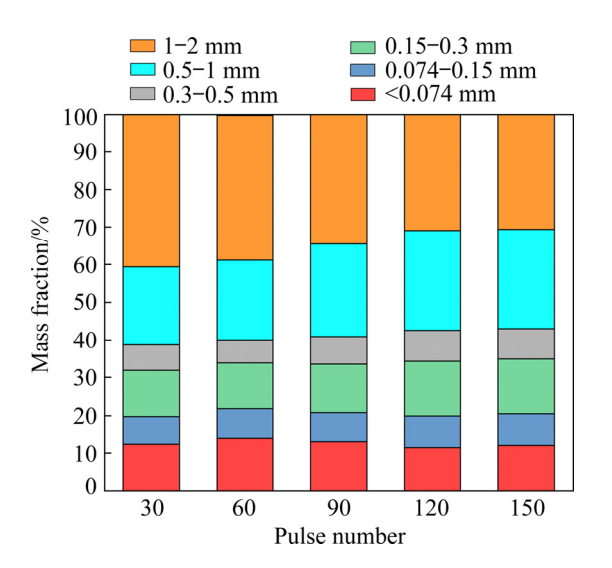
Pulse number	30	60	90	120	150
Energy/ $(kW \cdot h \cdot t^{-1})$	0.243	0.486	0.729	0.972	1.215

Fig. 5 indicated the mass fraction of HVPD products <2 mm increased with the increase of the pulse number. At pulse numbers of 30, 60, 90, 120, and 150, the mass fractions of products with size <2 mm were 12.16%, 22.44%, 33.93%, 40.01%, and 52.88%, respectively. The energy of HVPD increased with the increase of the pulse number. Therefore, the breakdown of ores was intensified with increasing the pulse number. However, the overheated phenomenon of facility was aggravated with a long discharge time. The quantity of heat was proportional to the pulse time. According to the Joule's law, the relationship between heat and pulse discharge time was shown in Eq. (3):

$$Q = I^2 Rt \tag{3}$$

where Q was the quantity of heat (J); I was the current (A); R was the resistance ( $\Omega$ ); t represented the pulse discharge time (s). More heat was produced by the longer pulse discharge time. Ultimately, the pulse number was determined to be 120.

The feed size distribution of the ball mill at different pulse numbers was shown in Fig. 6, which indicated that the mass fraction of products with size <1 mm increased with increasing the pulse number. At a pulse number of 150, the mass fractions of 1-2, 0.5-1, 0.3-0.5, 0.15-0.3,



**Fig. 6** Feed size distribution in ball mill at different pulse numbers

0.074–0.15, and <0.074 mm were 30.62%, 26.40%, 7.64%, 14.37%, 8.52%, and 12.13%, respectively. 3.1.3 Voltage

The effect of voltage on the comminution characteristic was investigated at a voltage varying from 22 to 31 kV, a pulse number of 120, and a spark gap spacing of 25 mm. The particle size distribution of HVPD products at different voltages was shown in Fig. 7. The energy was listed in Table 5.

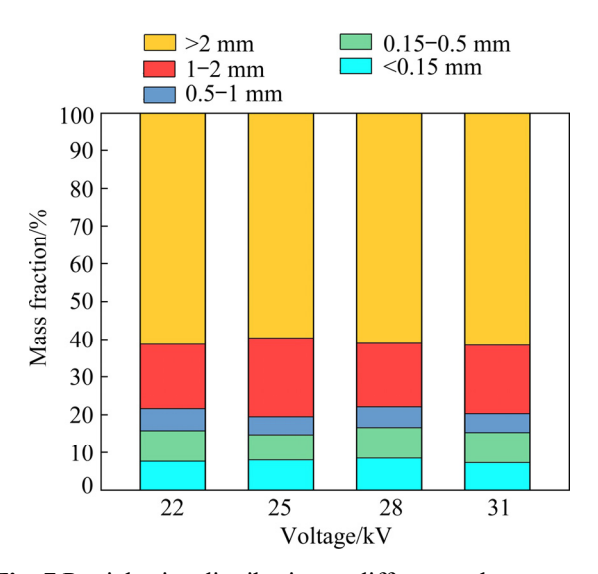


Fig. 7 Particle size distribution at different voltages

**Table 5** Energy of HVPD pre-treatment at different voltages

Voltage/kV	22	25	28	31	-
Energy/(kW·h·t <sup>-1</sup> )	0.565	0.729	0.914	1.121	

When the voltage was 22, 25, 28, and 31 kV, the mass fractions of products with sizes <2 mm were 38.70%, 40.01%, 38.90%, and 38.40%, respectively. The increase of voltage was beneficial to mineral fragmentation. However, the service life of the resistor and capacitor would be shortened by the excessive current produced via the higher voltage. Therefore, the appropriate voltage was confirmed to be 25 kV.

The feed size distribution in the ball mill at different voltages was shown in Fig. 8, which indicated that the mass fraction of products with size <1 mm at a voltage of 25 kV was the highest. At a voltage of 25 kV, the mass fractions of 1–2, 0.5–1, 0.3–0.5, 0.15–0.3, 0.074–0.15, and <0.074 mm were 30.92%, 26.55%, 8.09%, 14.33%, 8.44%, and 11.67%, respectively.

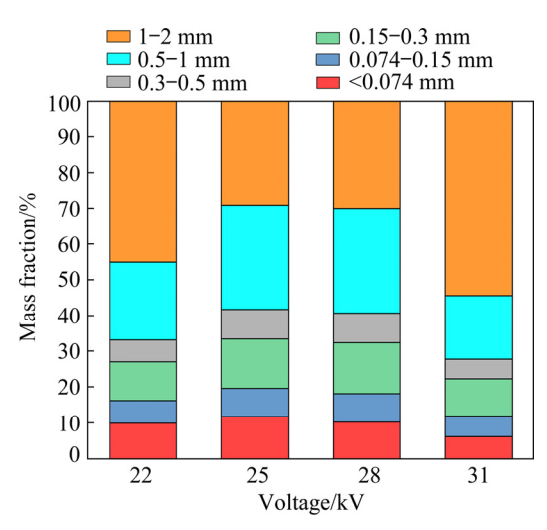


Fig. 8 Feed size distribution in ball mill at different voltage

## 3.2 Effect of grinding on HVPD comminution products

To characterize the superiority of HVPD, grinding experiments were operated at grinding pulp concentration of 70 wt.%, and grinding time 15, 30, 45, 60, and 75 s, respectively. The optimal parameters of HVPD were a spark gap spacing of 25 mm, a pulse number of 120, and a voltage of 25 kV. The feed particle size distribution of the ball mill was shown in Fig. 9. The mass fractions of HVPD products with size >1 mm and <0.074 mm were less than those of mechanical breakage. On the contrary, the mass fractions of HVPD products were higher than those of mechanical breakage in other size intervals.

To contrast the mechanical crushing and HVPD, grinding experiments of mechanical crushing products were operated at a grinding pulp

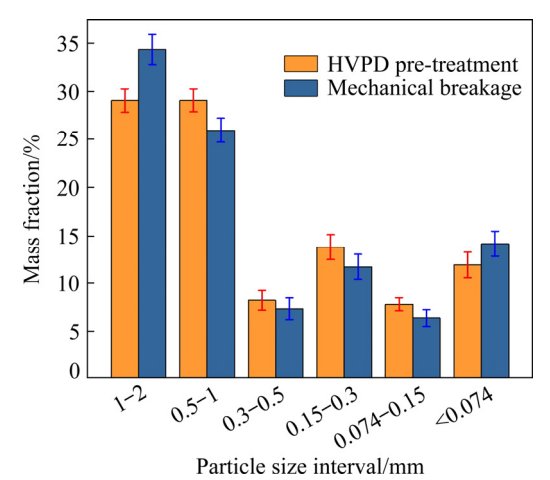
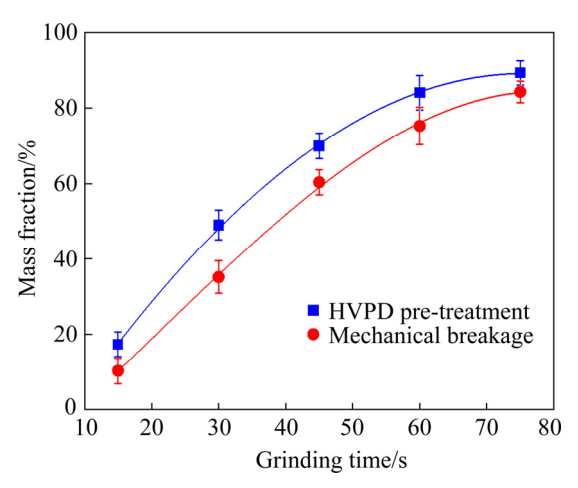


Fig. 9 Feed size distribution in ball mill via two breakage approaches

concentration of 70 wt.%, and grinding time of 15, 30, 45, 60, and 75 s, respectively. The ground products were sieved by a standard screen with a pore size of 0.074 mm, as shown in Fig. 10. At the grinding time of 30 s, the mass fractions of the ground products of HVPD and mechanical breakage products with sizes <0.074 mm were 49.08% and 35.23%; meanwhile, those were 89.44% and 84.43% at the grinding time of 75 s, respectively. The mass fractions of the ground products of HVPD with sizes <0.074 mm were higher than those of the ground products of mechanical breakage at the same grinding time.



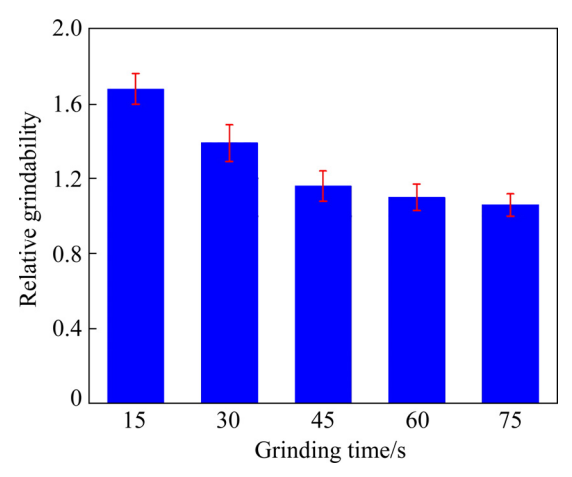
**Fig. 10** Grinding curves of breakage products with sizes <0.074 mm

Fig. 10 indicated that the grinding efficiency of galena ore was improved through the HVPD. The relative grindability experiments were conducted to ascertain the relationship between relative grindability and grinding time, and the experimental results were shown in Fig. 11. The relative grindability (K) was defined as follows:

$$K=M_p/M$$
 (4)

where  $M_p$  was the mass fraction of the ground product of HVPD breakage (<0.074 mm); M was the mass fraction of the ground product of mechanical crushing (<0.074 mm). Moreover,  $M_p$  and M were obtained at the same grinding time.

The relative grindability declined with the increase of grinding time. When the grinding time was 15, 30, 45, 60, and 75 s, the relative grindability was 1.68, 1.39, 1.16, 1.10, and 1.06, respectively, indicating that the positive impact of HVPD was weakened with the increase of grinding time.



**Fig. 11** Relationship between relative grindability and grinding time by HVPD

#### 3.3 Particle size distribution of ground products

The particle size distribution of ground products was investigated through the laser particle size analysis. The particle size distribution and cumulative particle size distribution of ground products were shown in Fig. 12 and Fig. 13, respectively. The relevant parameters of the particle size distribution of ground products were listed Table 6. As shown in Fig. 12, the peak value of volume fraction of HVPD product was higher than that of the mechanical breakage. Moreover, the distribution range of the HVPD ground product was narrower. The distribution of HVPD ground product was uniform owing to the selectivity breakage of HVPD, and more qualified granular particles were obtained via the HVPD breakage, which were more beneficial to separation operation. Figure 13 indicated that the gradient of the HVPD curve was higher than mechanical breakage curve. In other words, the distribution of HVPD ground products was more homogeneous.

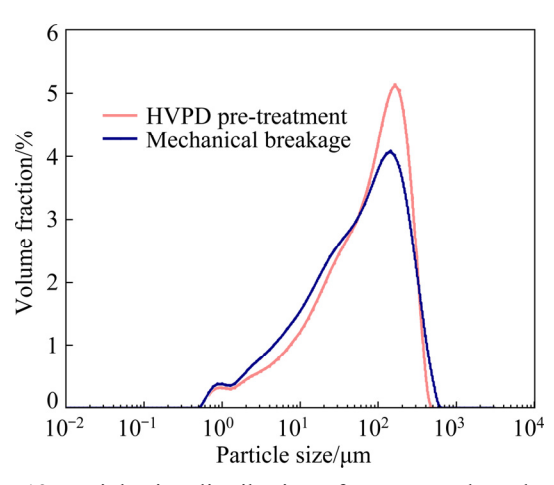


Fig. 12 Particle size distribution of two ground products

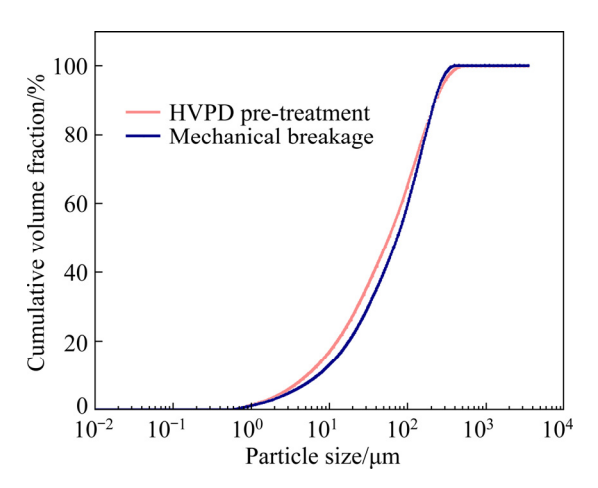


Fig. 13 Cumulative particle size distribution of two ground products

**Table 6** Relevant parameters for particle size distribution of two ground products

Treatment	D <sub>[4,3]</sub> / μm	Span	Consistency	D <sub>10</sub> / μm	$D_{50}$ / $\mu { m m}$	D <sub>90</sub> / μm
HVPD pre-treatment	94.6	3.612	1.119	5.9	63.2	234
Mechanical breakage	104	3.696	1.138	7.02	68.3	259

As listed in Table 6, the average particle sizes  $(D_{[4,3]})$  of HVPD and mechanical products were 94.6 and 104  $\mu$ m, respectively. The  $D_{50}$  values of two products were 63.2 and 68.3  $\mu$ m, while the  $D_{10}$  values were 5.9 and 7.02  $\mu$ m, respectively. The consistency represented the uniformity of particle distribution, and the consistency of HVPD product was 1.119, indicating that the HVPD product was more uniform than mechanical product. The size distribution span of HVPD product was less than that of mechanical product, which indicated that the distribution width of the former was narrower.

#### 3.4 Liberation of breakage products

To analyze the superiority of HVPD pretreatment on the minerals liberation, the mechanical breakage products and the HVPD samples obtained at a spark gap spacing of 25 mm, a pulse number of 120, and a voltage of 25 kV were prepared for liberation experiments, as shown in Fig. 14. The intergrowth characteristics of breakage samples under optical microscope were shown in Fig. 15. Figure 14 indicated that the proportion of galenapyrite, galenapague, and galenapyrite—gangue in the HVPD products were 13.11%, 3.96%, and

18.52%, respectively. The proportions of galenapyrite, galena-gangue, and galena-pyrite-gangue in the mechanical breakage products were 13.22%, 5.46%, and 55.17%, respectively. More importantly, the proportions of galena in two breakage products were 47.85% and 23.28%, which indicated that the liberation of breakage products was enhanced via the HVPD. Due to the dielectric constant difference between metallic minerals and gangue, the induced electric-field was generated at the interface of minerals to promote the plasma channel developing along with the minerals interface. Meanwhile, the impact wave and thermal expansion stress were generated to accelerate the minerals separating along with the interface [24-26]. Therefore, the liberation characteristics of the products were enhanced through the selective breakage of HVPD.

#### 3.5 Microstructure of breakage products

#### 3.5.1 BET specific surface area

A high-temperature environment was generated on account of the plasma channel explosion at the mineral interface, and several fused traces and a lot of gases were produced. At the high-temperature molten state, numerous pores were generated on the mineral surface through these gases [27–29]. The BET analysis of breakage products with size <2 mm was performed to investigate the microstructure of the HVPD and

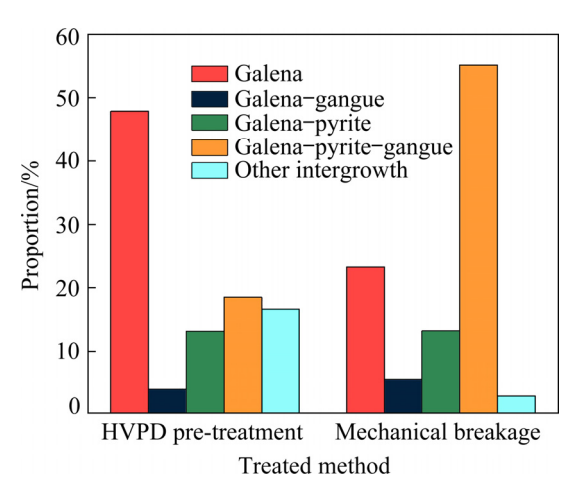


Fig. 14 Liberation characteristics of two breakage products

mechanical products, as shown in Fig. 16 and Fig. 17.

The N<sub>2</sub> physisorption isotherms of HVPD and mechanical products were exhibited in Fig. 16. The N<sub>2</sub> adsorption capacity of mechanical breakage product was lower than that of HVPD products, indicating that the number of pores in HVPD product was less. According to the IUPAC classification, the N<sub>2</sub> adsorption—desorption isotherm was a typical type IV isotherm. Since the average pore diameters of HVPD and mechanical product were 5.04 and 4.50 nm, respectively, the pores belonged to mesopores.

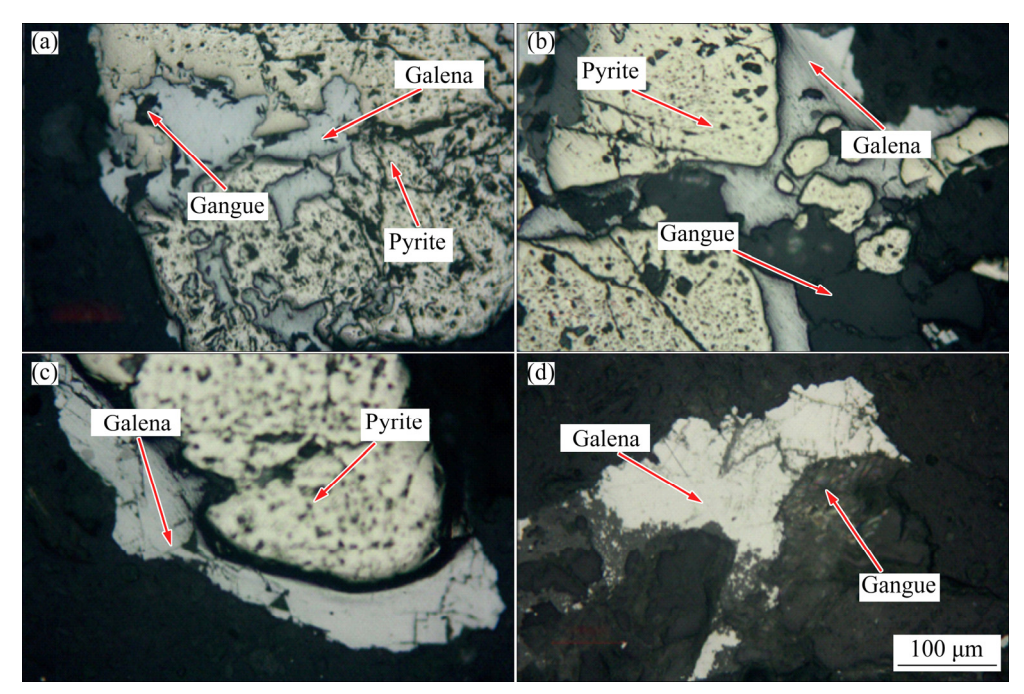


Fig. 15 Optical morphologies of breakage products: (a, b) Galena, gangue and pyrite; (c) Galena and pyrite; (d) Galena and gangue

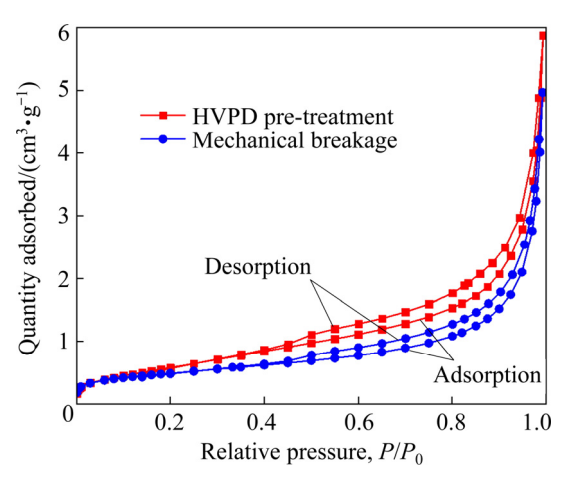


Fig. 16 N<sub>2</sub> adsorption—desorption isotherms of breakage products

The pore diameter distribution of two breakage products in adsorption and desorption processes was shown in Fig. 17. Figures 17(b, d) indicated that the largest pore volume was improved by the HVPD. From Table 7, the BET surface area, BJH

adsorption pore volume, BJH desorption pore volume, and average pore size were enhanced via the HVPD. Due to the transformation of ore microstructure, the mechanical properties of the ores were weakened and the grinding efficiency was enhanced through the HVPD.

#### 3.5.2 SEM results

The influence of HVPD on the micromorphology of ores was studied by SEM and EDS analyses, as shown in Figs. 18 and 19. On account of the disparate principles of mechanical breakage and HVPD, the surfaces of breakage products exhibited various micro-morphologies. As shown in Figs. 18(a, b), since mechanical impact mainly overcame the compressive stress in ores, there were no distinct grain-boundary cracks in mechanical breakage products.

Figures 18(c, d) and Fig. 19 indicated that the grain-boundary cracks were generated at the interface of galena and dolomite on account of the difference of dielectric constants. From Fig. 19, the

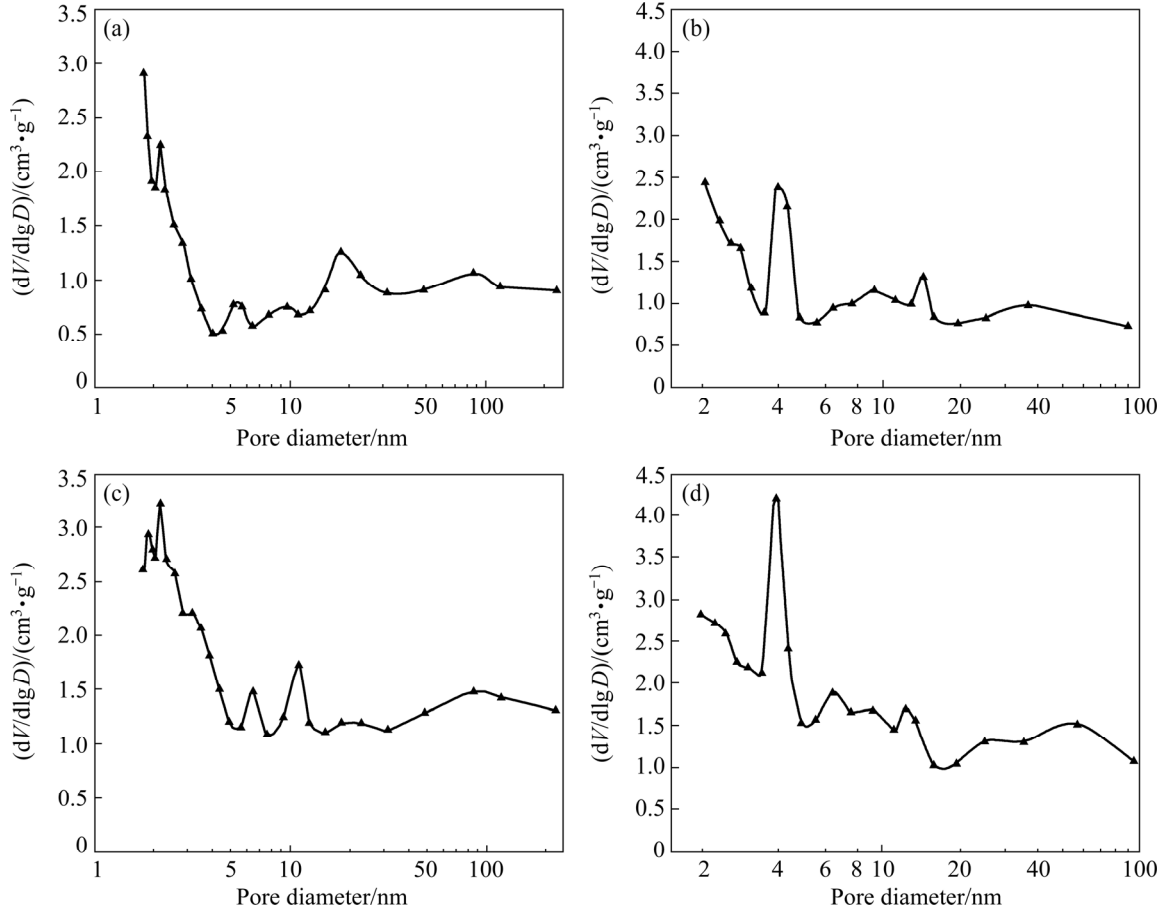


**Fig. 17** Pore diameter distributions of breakage products in BJH mode: (a) Mechanical breakage products in BJH adsorption process; (b) Mechanical breakage products in BJH desorption process; (c) HVPD products in BJH adsorption process; (d) HVPD products in BJH desorption process; (V is pore volume, and D is pore diameter)

**Table 7** Detailed results of BET analysis

Product	BET specific surface area/(m <sup>2</sup> ·g <sup>-1</sup> )	BJH adsorption pore volume/(cm <sup>3</sup> ·g <sup>-1</sup> )	BJH desorption pore volume/(cm <sup>3</sup> ·g <sup>-1</sup> )	Average pore size/nm
HVPD pre-treatment	1.4644	0.003407	0.003558	5.04
Mechanical breakage	1.1732	0.002263	0.002316	4.50

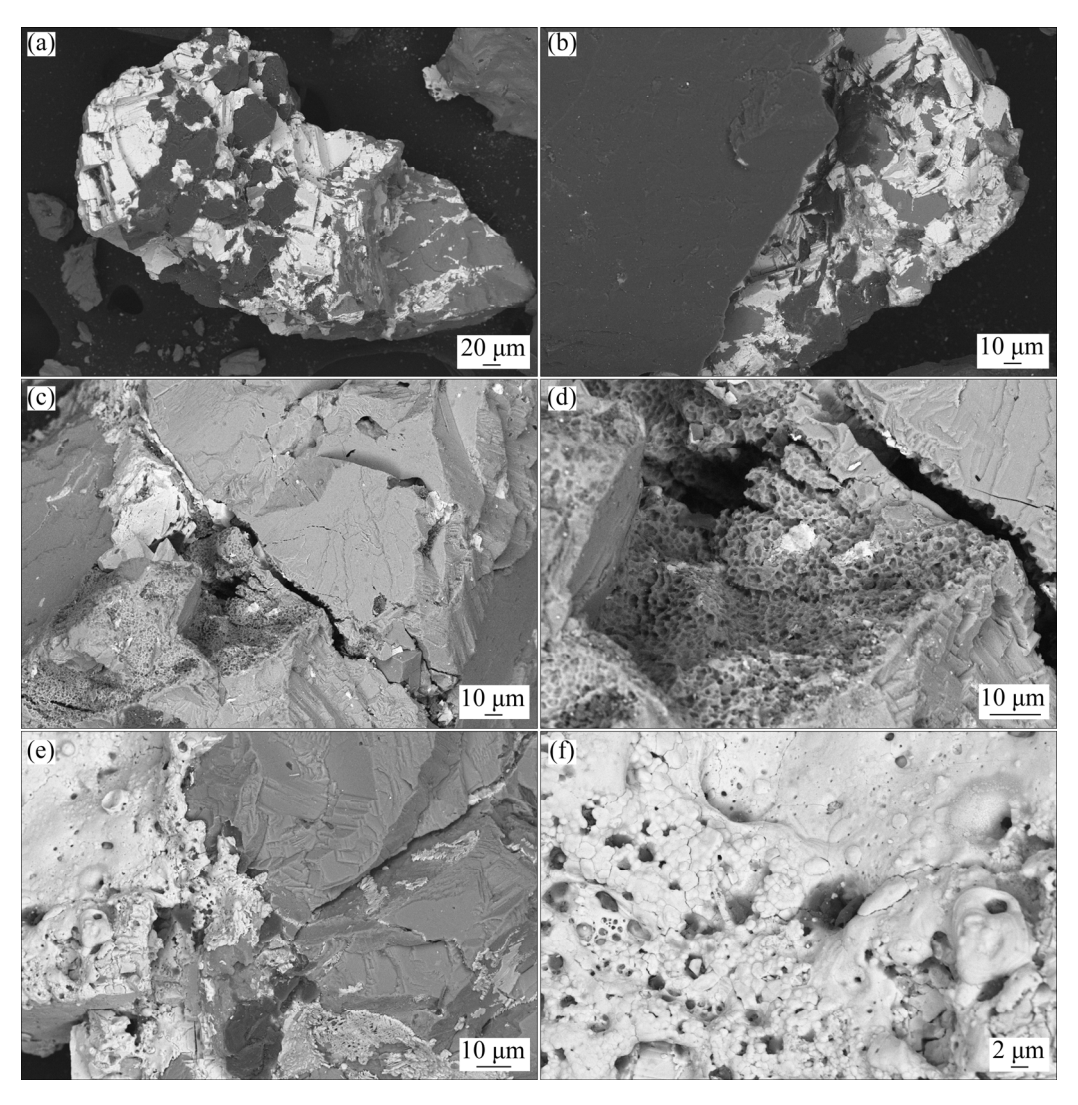


Fig. 18 SEM images of two breakage products: (a, b) Mechanical breakage products; (c-f) HVPD pre-treatment products

elements at Points A and C were mainly lead, indicating that the minerals were galena. On the contrary, dolomite and quartz were the main minerals at Points B and D. The phenomenon of liberation generated at the interface of metallic and gangue minerals was known as the selective breakage. In other words, the grain-boundary cracks extended along the interface of different mineral components. Ultimately, the selective breakage was generated based on the combined effect of plasma channel, high-temperature environment, impact wave, and thermal expansion [30–34].

Moreover, the temperature of the plasma channel rose rapidly due to Joule's law. The thermal expansion effect was generated at the mineral interface, and the grain-boundary cracks were generated owing to the stress of different minerals. As shown in Figs. 18(d-f), the pore structure was observed on the surface of metallic mineral in HVPD products. On account of the high-temperature of the plasma channel, the minerals were melted by the Joule heat. Meanwhile, the gases such as H<sub>2</sub>S, SO<sub>2</sub>, and H<sub>2</sub>O were released to produce the stomatal traces [17].

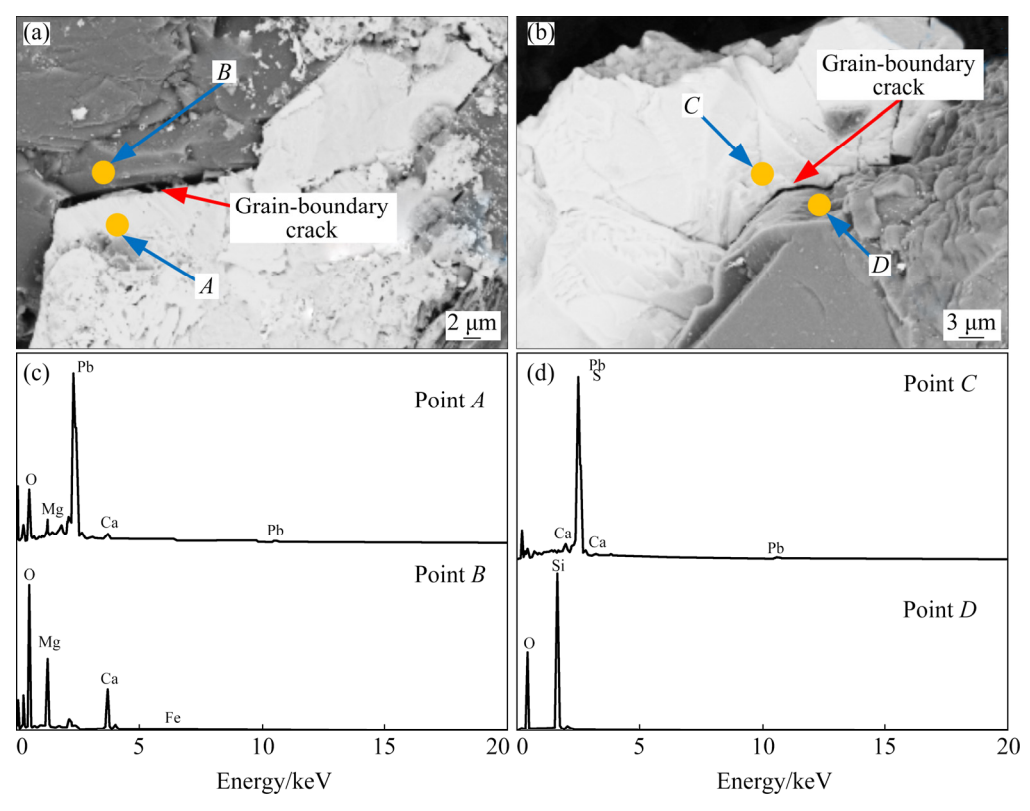


Fig. 19 SEM images (a, b) and EDS maps (c, d) of grain-boundary cracks of HVPD pre-treatment products

#### 4 Conclusions

(1) The useful element of the ore sample was lead. The main impurities included CaO (18.55%), SiO<sub>2</sub> (16.18%), and MgO (13.42%). MLA analysis suggested that the metallic minerals were galena (5.06%), pyrite (17.57%), magnetite, chalcopyrite, freibergite, and boulangerite. The gangue minerals consisted of dolomite (57.78%), quartz (11.38%), mica, calcite, chlorite, and apatite. The galena and pyrite were wrapped by dolomite and quartz, respectively. The disseminated grains of galena, pyrite, dolomite, quartz, and mica were coarse. The disseminated grains of boulangerite and freibergite were fine particles.

(2) At a spark gap spacing of 25 mm, a pulse number of 120, and a voltage of 25 kV, the mass fractions of HVPD products with sizes of 1–2, 0.5–1, 0.3–0.5, 0.15–0.3, 0.074–0.15, and <0.074 mm were 30.92%, 26.55%, 8.09%, 14.33%, 8.44%, and 11.67%, respectively. The mass fractions with sizes <0.074 mm in ground products were increased by the HVPD. Meanwhile, the relative grindability declined with the increase of grinding time, which indicated that the superiority of HVPD was weakened. The ground products of

HVPD were distributed more homogeneously than the ground products of mechanical crushing.

(3) Due to the dielectric properties difference between metallic minerals and gangue, the liberation of breakage products was improved by 24.57% through the HVPD. The BET specific surface area, BJH adsorption pore volume, BJH desorption pore volume, and average pore size were enhanced via the HVPD. On account of the selective breakage effect of HVPD breakage, the obvious grain-boundary breakage was observed under SEM and EDS. Moreover, several stomatal traces were observed in the HVPD products.

#### **Acknowledgments**

The authors are grateful for the financial supports from the National Natural Science Foundation of China (No. 51974063), the Fundamental Research Funds for the Central Universities of China (No. N180104016), and the China Postdoctoral Science Foundation (No. 2020M670783).

#### References

[1] ZHANG Ye, LIU Run-qing, SUN Wei, WANG Li, DONG

- Yan-hong, WANG Chang-tao. Electrochemical mechanism and flotation of chalcopyrite and galena in the presence of sodium silicate and sodium sulfite [J]. Transactions of Nonferrous Metals Society of China, 2020, 30: 1091–1101.
- [2] ZHOU Wen-tao, HAN Yue-xin, SUN Yong-sheng, YANG Jin-lin, MA Shao-jian. Multi-scale impact crushing characteristics of polymetallic sulphide ores [J]. Transactions of Nonferrous Metals Society of China, 2019, 29: 1929–1938.
- [3] SUN Yong-sheng, ZHOU Wen-tao, HAN Yue-xin, LI Yan-jun. Effect of different additives on reaction characteristics of fluorapatite during coal-based reduction of iron ore [J]. Metals, 2019, 9: 923.
- [4] ZHANG Xiao-long, HAN Yue-xin, SUN Yong-sheng, LI Yan-jun. Innovative utilization of refractory iron ore via suspension magnetization roasting: A pilot-scale study [J]. Powder Technology, 2019, 352: 16–24.
- [5] TANG Zhi-dong, GAO Peng, SUN Yong-sheng, HAN Yue-xin, LI Er-lei, CHEN Jia, ZHANG Ya-hui. Studies on the fluidization performance of a novel fluidized bed reactor for iron ore suspension roasting [J]. Powder Technology, 2020, 360: 649–657.
- [6] YUAN Shuai, ZHOU Wen-tao, HAN Yue-xin, LI Yan-jun. Efficient enrichment of low-grade refractory rhodochrosite by preconcentration-neutral suspension roasting-magnetic separation process [J]. Powder Technology, 2020, 361: 529-539.
- [7] YU Jian-wen, HAN Yue-xin, LI Yan-jun, GAO Peng. Effect of magnetic pulse pre-treatment on grindability of a magnetite ore and its implication on magnetic separation [J]. Journal of Central South University of Technology, 2016, 23: 3108-3114.
- [8] ERIC W, SHI Feng-nian, MANLAPIG E. Pre-weakening of mineral ores by high voltage pulses [J]. Minerals Engineering, 2011, 24: 455–462.
- [9] MENG Yang, YAN Yu-xin, JIANG Peng, ZHANG Min, OLADEJO J, WU Tao, PANG Cheng-heng. Investigation on breakage behaviour of oil shale with high grinding resistance: A comparison between microwave and conventional thermal processing [J]. Chemical Engineering & Processing: Process Intensification, 2020, 151: 107909.
- [10] BUTTRESS A J, RODRIGUEZ J M, URE A, FERRARI R S, DODDS C, KINGMAN S W. Production of high purity silica by microfluidic-inclusion fracture using microwave pretreatment [J]. Minerals Engineering, 2019, 131: 407–419.
- [11] HAN Yue-xin, LIU Lei, YUAN Zhi-tao, WANG Ze-hong, PATRICK Z. Characteristic comparison of low-grade hematite product characteristics in a high pressure grinding roller and jaw crusher [J]. Minerals & Metallurgical Processing, 2012, 29: 75–80.
- [12] QIN Yong-hong, HAN Yue-xin, GAO Peng, LI Yan-jun, YUAN Shuai. Pre-weakening behavior of magnetite quartzite based on high-voltage pulse discharge [J]. Minerals Engineering, 2021, 160: 106662.
- [13] ANDRES U. Development and prospects of mineral liberation by electrical pulses [J]. International Journal of Mineral Processing, 2010, 97: 31–38.
- [14] BRU K, TOUZE S, AUGER P, DOBRUSKY S, TIERRIE J, PARVAZ D B. Investigation of lab and pilot scale electric-

- pulse fragmentation systems for the recycling of ultrahigh performance fibre-reinforced concrete [J]. Minerals Engineering, 2018, 128: 187–194.
- [15] PARKER T, SHI F N, EVANS C, POWELL M. The effects of electrical comminution on the mineral liberation and surface chemistry of a porphyry copper ore [J]. Minerals Engineering, 2015, 82: 101–106.
- [16] MARTELLOA E D, BERNARDISB S, LARSENC R B, TRANELLA G, SABATINOA M D, ARNBERGA L. Electrical fragmentation as a novel route for the refinement of quartz raw materials for trace mineral impurities [J]. Powder Technology, 2012, 224: 209–216.
- [17] ZHAO Peng-fei, Guo Jun-wei, YAN Guang-hui, ZHU Guang-qing, ZHU Xiang-nan, ZHANG Zhen-xing, ZHANG Bo. A novel and efficient method for resources recycling in waste photovoltaic panels: High voltage pulse crushing [J]. Journal of Cleaner Production, 2020, 257: 120442.
- [18] CHANTURIYA V A, BUNIN I Z, KOVALEV A T. The role of gas outflow from nanosecond breakdown channels in the electric-pulse discharge disintegration of sulfide minerals [J]. Bulletin of the Russian Academy of Sciences: Physics, 2010, 74: 663–666.
- [19] GAO Peng, YUAN Shuai, HAN Yue-xin, LI Yan-jun, CHEN Hong-yun. Experimental study on the effect of pretreatment with high-voltage electrical pulses on mineral liberation and separation of magnetite ore [J]. Minerals, 2017, 7: 153.
- [20] SHI Feng-nian, ZUO Wei-ran, MANLAPIG E. Characterisation of pre-weakening effect on ores by high voltage electrical pulses based on single-particle tests [J]. Minerals Engineering, 2013, 50-51: 69-76.
- [21] ZUO Wei-ran, SHI Feng-nian. A  $t_{10}$ -based method for evaluation of ore pre-weakening and energy reduction [J]. Minerals Engineering, 2015, 79: 212–219.
- [22] DIAO Zhi-jun. Study on mechanism of fragmentation of waste printed circuit board by high voltage pulse [D]. Xuzhou: China University of Mining and Technology, 2013. (in Chinese).
- [23] DUAN Chen-long, DIAO Zhi-jun, ZHAO Yue-min, HUANG Wei. Liberation of valuable materials in waste printed circuit boards by high-voltage electrical pulses [J]. Minerals Engineering, 2015, 70: 170–177.
- [24] ZHAO Yue-min, ZHANG Bo, DUAN Chen-long, CHEN Xia, SUN Song. Material port fractal of fragmentation of waste printed circuit boards (WPCBs) by high-voltage pulse [J]. Powder Technology, 2015, 269: 219–226.
- [25] ERIC W, SHI F N, MANLAPIG E. Mineral liberation by high voltage pulses and conventional comminution with same specific energy levels [J]. Minerals Engineering, 2012, 27: 28–36.
- [26] HUANG Wei, SHI Feng-nian. Selective breakage of mineralised synthetic particles by high voltage pulses. Part 1: Metalliferous grain-induced breakage in a two-particle paired system [J]. Minerals Engineering, 2019, 134: 261–268.
- [27] HUANG Wei, SHI Feng-nian. Improving high voltage pulse selective breakage for ore pre-concentration using a multiple-particle treatment method [J]. Minerals Engineering, 2018, 128: 195–201.
- [28] YAN Guang-hui, ZHANG Bo, LV Bo, ZHU Guang-qing,

- ZHU Xiang-nan, ZHAO Yue-min. Enrichment of chalcopyrite using high-voltage pulse discharge [J]. Powder Technology, 2018, 340: 420–427.
- [29] YAN Fa-zhi, LIN Bai-quan, XU Jiang, WANG Yi-han, ZHANG Xiang-liang, PENG Shou-jian. Structural evolution characteristics of middle-high rank coal samples subjected to high-voltage electrical pulse [J]. Energy & Fuels, 2018, 32: 3263–3271.
- [30] HUANG Wei, SHI Feng-nian, JOKOVIC V. A method to determine the minimum quantity of ore sample required for laboratory scale study of ore pre-concentration by high voltage pulses [J]. Minerals Engineering, 2018, 127: 247–255.
- [31] ZHU Chuan-jie, LU Xi-miao, LIN Bai-quan, YAN Fa-zhi, GUO Chang, HONG Yi-du, ZHANG Xiang-liang.

- Experimental study on the microscopic characteristics affecting methane adsorption on anthracite coal treated with high-voltage electrical pulses [J]. Adsorption Science & Technology, 2018, 36: 170–181.
- [32] ERIC W, SHI Feng-nian, MANLAPIG E. Factors affecting electrical comminution performance [J]. Minerals Engineering, 2012, 34: 48–54.
- [33] ANDRES U. Development and prospects of mineral liberation by electrical pulses [J]. International Journal of Mineral Processing, 2013, 97: 31–38.
- [34] DUAN Chen-long, HAN Jun, ZHAO Shen, GAO Zhong-lin, QIAO Jin-peng, YAN Guang-hui. The stripping effect of using high voltage electrical pulses breakage for waste printed circuit boards [J]. Waste Management, 2018, 77: 603-610.

### 一种高压电脉冲粉碎方铅矿石新技术

秦永红<sup>1,2</sup>, 高鹏<sup>1,2</sup>, 袁帅<sup>1,2</sup>, 张宁豫<sup>1,2</sup>, 韩力仁<sup>1,2</sup>

- 1. 东北大学 资源与土木工程学院, 沈阳 110819;
- 2. 难选铁矿资源高效开采技术国家地方联合工程研究中心, 沈阳 110819

摘 要:为研究方铅矿的粉碎特性,提出一种高压脉冲放电(HVPD)新技术。其最优的实验参数如下:火花隙间距 25 mm、脉冲数 120、电压 25 kV。高压电脉冲提高研磨产品中粒度小于 0.074 mm 的质量分数。同时,随着研磨时间的延长,相对可磨性下降,说明 HVPD 的优越性减弱。高压电脉冲粉碎产物比机械粉碎产物分布均匀。高压电脉冲使破碎产物的单体解离度提高 24.57%。此外,采用高压电脉冲粉碎产品的 BET 比表面积、孔体积和平均孔径得到提高。扫描电镜(SEM)和 X 射线能谱(EDS)分析表明,高压电脉冲产物中存在明显的晶界断裂和气孔痕迹。

关键词: 方铅矿石; 高压脉冲放电; 解离; 显微组织; 晶界断裂

(Edited by Wei-ping CHEN)